

## Design Spectra and Phase Spectrum Modeling to Simulate Design Earthquake Motions: A Case study through Design Standards of Railway Facilities in Japan

Tadanobu SATO <sup>1)</sup>, Yoshitaka MURONO <sup>2)</sup>, Hai-Bo WANG <sup>2)</sup>, Akihiko NISHIMURA <sup>2)</sup>

<sup>1)</sup> Disaster Prevention Research Institute, Kyoto University, Kyoto, Japan

<sup>2)</sup> Railway Technical Research Institute, Tokyo, Japan

(Received for 14 Mar., 2002)

### ABSTRACT

Design earthquake motions often are defined by response spectra. We introduce three types of design spectra given in the *Seismic Design standards for Railway Facilities* (1999). Both the amplitude and phase characteristics of earthquake motion provide key information needed to evaluate the aseismic capacity of designed structures. We present a simple method for modeling the phase characteristic of earthquake motion based on group delay time and wavelet analysis. First the phase spectrum is modeled near the source region. Second we develop a method to model the phase spectrum for the inter-plate earthquakes. Existing data sets on observed earthquake motions and wavelet analysis then are used to calculate the group delay time of each earthquake motion on each compact support of Meyer's analyzing wavelet. Regression equations for the mean group delay time and standard deviation on each compact support are obtained as functions of the earthquake's magnitude and epicentral distance. Simulating sample phase spectra earthquake motions compatible with the design response spectra then are simulated, and their characteristics are investigated using ductility demand spectra.

### 1. INTRODUCTION

Because of the severe damage done to urban facilities by the 1995 Hyogoken Nambu earthquake, many Japanese earthquake design standards have been revised. After two years of activity, a committee brought together to revise the aseismic design standards for railway facilities issued "Design Standards for Railway Facilities: commentaries on aseismic design". After introducing three types of design response spectra defined in the Design Standards for Japanese Railway Facilities we here develop methods to simulate phase spectra to be used for generating design earthquake motions.

### 2. EARTHQUAKE MOTION AT THE ENGINEERING BASE LAYER

Earthquakes that occur near the Japanese archipelago are classified as intra- and inter-plate earthquakes. The Pacific and Philippine plates move, respectively, in the west and north-west directions, and both are subducted along the Pacific periphery of the Japanese archipelago. The associated tectonic forces cause magnitude 8 class earthquakes. The return period of earthquake occurrence in the same area ranges from several tens to two hundred years. Recent inter-plate earthquakes are shown in Figure 1.

In contrast, the average return period of an intra-plate earthquake having a magnitude larger than 7 at a certain active fault is several thousands years. If, however, such an event occurs near a densely populated urban area severe damage is done to structures. Moreover, the average occurrence rate of intra-plate earthquakes of a magnitude larger than 6.8 within the Japanese archipelago is

about 12 years (Rika Nenpyo 2001) <sup>1)</sup>. The intensities of intra-plate earthquakes therefore were taken into account when establishing the design standards, as were those of inter-plate earthquakes (JSCE 1996) <sup>2)</sup>.

When establishing design standards, the design earthquake intensity must be defined through risk analyses at the design point. Although an intensive survey of inland active faults was made after the 1995 Hyogoken Nambu earthquake, accuracy in estimating the return period of earthquakes caused by those faults is not good enough to use for design standards. Therefore, the positions of all the detected inland active faults only have been used to define design earthquake intensity in the new design standards. A flow chart in Figure 2 shows how design earthquake motion is defined. This motion is defined at the engineering base ground where the N values of the standard penetration test are more than 50 or the shear wave velocity is more than 350 m/sec. The intensity of the design earthquake motion is defined by the response spectrum.

Spectrum I is obtained by taking into account the inter-plate fault activities that cause magnitude 8 class earthquakes. Because the epicentral distances of these earthquakes are more than 40 km, the defined spectrum level also envelopes spectra of the near source earthquake motions caused by M6.5 class intra-plate earthquakes. This is the minimum intensity level required in the seismic design standards.

Spectrum II is obtained from regression analysis based on observed earthquake motions caused by intra-plate earthquakes. Methods to simulate strong earthquake motions based on theoretical fault models have become popular in the field of civil engineering. The spectrum obtained by theoretically taking into account

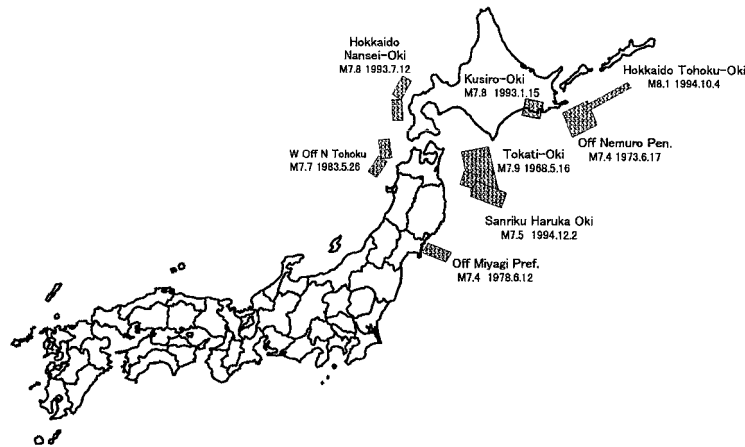


Fig. 1 Recent interplate earthquakes in Japan

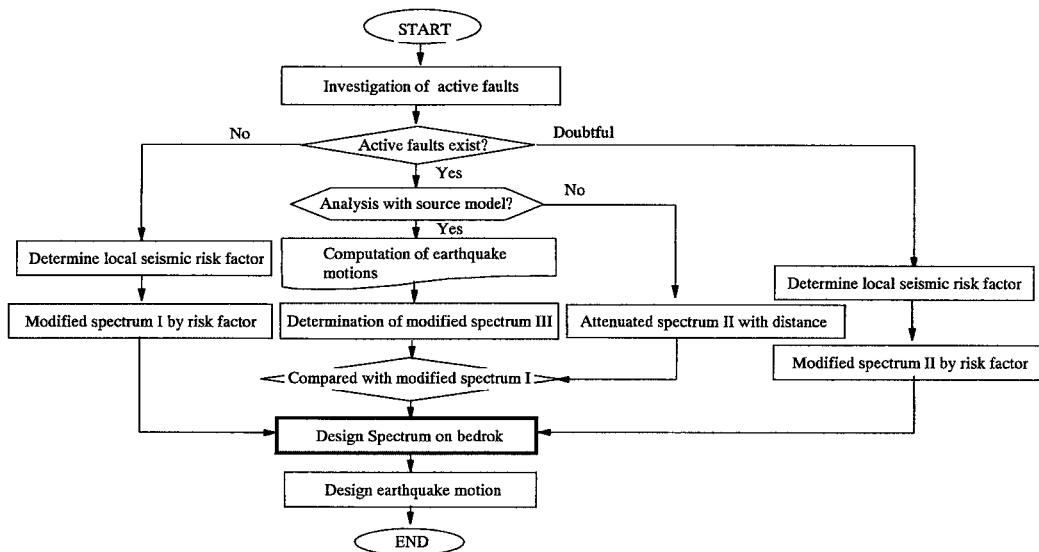


Fig. 2 Flowchart showing design seismic motion determination

the fault mechanism is called spectrum III.

Areas in which there is high probability of existing active faults whose detection is not easy due to deep alluvial and diluvial deposits and metropolitan areas with complicated crustal structures are classified as areas of high uncertainty of fault existence. In these areas the design earthquake intensity is defined by spectrum II modified by a regional correction factor.

### 3. DESIGN RESPONSE SPECTRA<sup>3)</sup>

#### 3.1 Spectrum II (for intra-plate earthquakes)

##### (1) Near Source Earthquake Motion Records

Spectrum II is defined stochastically by the use of response spectra calculated from observed near source earthquake motions. We collected observed earthquake motions recorded on hard ground to define design response spectrum free from the effect of topological condition and ground irregularity as well as amplification of soft surface layers. Table 1 gives near source earthquake motions with maximum accelerations of more than 100gal observed on hard ground during the 1995 Hyogoken Nambu earth-

quake (M7.2), Coyote Lake earthquake (1979, M5.9), Loma Prieta earthquake (1989, M7.1), Landers earthquake (1992, M7.5) and Northridge earthquake (1994, M6.7). Although collected earthquake motions are mainly from the earthquakes occurred in the United States except the 1995 Hyogoken Nambu earthquake we assumed that there is no distinguishable difference between the U.S. and Japanese earthquake motions. Their acceleration response spectra are shown in Figure 3.

The observed records at Tarzana during the Northridge earthquake and those at the Kobe Power Transfer Station, as well as at the Takarazuka Station of the Japan Railway Company, during the 1995 Hyogoken Nambu earthquake were not used because effects of topological conditions were reported to be large. Acceleration response spectra calculated from these observed earthquake motions are shown by dotted lines in Figure 3.

Spectra scattering is very extensive. It originates from uncertainty about the 1) source mechanism, 2) transmitting path, 3) geographical structure and 4) local soil condition. To reduce scattering, the calculated response spectra levels are corrected by the proposed attenuation relationship.

Table 1. Near-source seismic records from recent earthquakes

No	Earth-quake	Name of seismic record	Max. Acc. (gal)		Latitude	Longitude	Equivalent hypocentral distance	Shortest Distance to Fault	Ground level of observation
			NS	EW					
1	Hyogoken-Nanbu	Port Island	679.8	302.6	34.670	135.208	11.64	3.24	GL-83
2		Takasago Power Station	86.0	109.3	34.753	134.783	32.75	27.08	GL-100
3		SGK.KansaiElec.Power Co.	293.9	319.8	34.743	135.442	34.57	24.65	GL-97.0
4		Roko(Kobe University)	272.0	306.5	34.725	135.240	14.99	6.90	GL-9.5
5		Inagawa	185.3	200.4	34.836	135.427	38.03	25.03	GL-30
6		Great Bridge of East Kobe	445.9	425.3	34.707	135.296	20.00	12.38	GL-33
7		Takarazuka	683.6	600.9	34.809	135.344	29.93	16.88	GL0.0
8		New Kobe substation	510.7	584.2	34.731	135.250	16.52	7.53	GL0.0
9	Covote Lake	San Ysidro	314.6	408.8	37.026	121.484		1.0	GL0.0
10	Loma Prieta	Santa Cruz UCSC	433.1	401.5	37.00	122.06	18.01	12.19	GL0.0
11		Gilroy#1-Gavilan Coll.	426.6	433.6	36.973	121.572	26.56	12.21	GL0.0
12	Landers	Joshua Tree fire station	268.3	278.4	34.131	116.314	16.90	10.79	GL0.0
13		Tarzana Cedar Hill	970.7	1744.5	34.160	118.534	20.63	17.87	GL0.0
14	Northridge	Pacoima Kegel Canyon	424.2	295.2	34.288	118.375	18.73	8.98	GL0.0

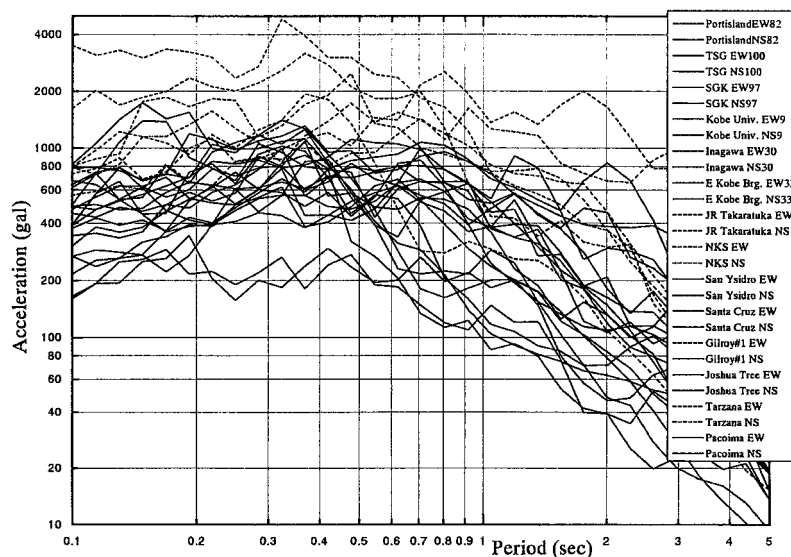


Fig. 3 Acceleration response spectra of observed records at near source regions of inland earthquakes

## (2) Response Spectra Adjustment Using the Attenuation Relation

There are several attenuation relationships of the acceleration response spectrum that take into account the earthquake source extent. An attenuation relationship that uses the shortest distance to the earthquake fault, proposed by Fukushima (1994) <sup>4)</sup>, is given by

$$\log S(T) = a_1(T)M_w^2 - a_2(T)M_w + b(T) \cdot R - \log(R + 0.025 \times 10^{0.42M_w}) + \sum c_j(T)I_j \quad (1)$$

An attenuation relationship that uses the equivalent hypocentral distance was proposed by Ohno(1994) <sup>5)</sup>;

$$\log S(T) = a(T)M_w - \log X_{eq} - b(T)X_{eq} + c(T) + \Delta s(T) \quad (2)$$

$$X_{eq}^{-2} = \frac{\sum_{i=1}^N d_i^2 X_i^{-2}}{\sum_{i=1}^N d_i^2}$$

in which  $T$  is the period,  $M_w$  the moment magnitude,  $R$  the shortest distance to the earthquake fault,  $I_j$  the correction factor,  $X_{eq}$  the equivalent hypocentral distance,  $N$  the number of subdivided elements of the earthquake fault, and  $d_i$  and  $X_i$  respectively are the dislocation on a subdivided element and the hypocentral distance to

that element.

The shortest distance from an observation point to the earthquake fault and the equivalent hypocentral distance are shown in Table 1. We used fault models obtained from the publications of Wang et al. (1997) <sup>6)</sup> to calculate these values.

Inland earthquake fault planes usually are vertical, the fault bottoms being 15-20km from the ground surface, depending on the thickness of the earth's crust. An increase in earthquake magnitude increases the length of the earthquake fault. The intensity of earthquake ground motion near a fault region, however, is not proportional to earthquake magnitude because the effect of rupture energy released on a fault plane distant from the observation point decreases with an increase in the distance to the rupture point. The affected area becomes large as earthquake magnitude increases, but ground motion intensity asymptotes to a constant value for points with the same shortest distance to the fault in the near source region. To clarify the characteristics of earthquake motion just above a fault, the calculated response spectra from observed earthquake motions were adjusted to those at an equivalent hypocentral distance, 12km, from the fault (Figure 4). The average adjusted response spectra level becomes high, but almost all these spectra are bounded by 2000 gal, except those calculated using

Table 2. Seismic records from recent interplate earthquakes in Japan

Earthquake	No	Recorded site	Latitude	Longitude	Hypocentral distance (km)	Equivalent Hypocentral distance (km)	Closest Distance to Fault (km)	Position of seismometer
Tokachi-Oki (May 16,1968)	1	Hachinohe	40.55	141.483	179.4	130	88.6	GL
Off Nemuro Pen. (June 17,1973)	2	Otanoshike Brg.	43.0083	144.271	136.9	163.7	109.7	GL
Off Miyagi Pref. (June 12,1978)	3	Kaihoku Brg.	38.445	141.313	81.6	70.2	56.5	GL
	4	Ofunato-Bochi	39.00	141.733	101.7	86.8	71.6	GL
W off N Tohoku (May 26,1983)	5	Kamitorizawi Brg.	42.1014	140.563	231	190.8	144.5	GL
Kusiro-Oki (Jan. 15, 1993)	6	Urakawa	42.158	142.781	151.6	174.4	149.1	GL
	7	Hanasaki Port	43.2800	145.589	109.4	156.4	131.3	GL
	8	Tokachi Port	42.2889	143.324	106.5	141.7	121.8	GL
	9	Hiroo Brg.	42.2792	143.319	107.5	142.4	122.4	GL
	10	Otanoshike Brg.	43.0083	144.271	19.8	105.2	100.1	GL
Hokkaido Nansei-Oki (July 12,1993)	11	Chiyoda Brg.	42.9197	143.389	81.5	123.3	108.2	GL
	12	Muroran Port	42.3167	140.967	153.3	149.0	129.3	GL
Hokkaido Tohoku-Oki (Oct 4,1994)	13	Kamitorizawi Brg.	42.1014	140.563	124.6	120.1	91.4	GL
	14	Hanasaki Port	43.2800	145.589	168.4	123	58.5	GL

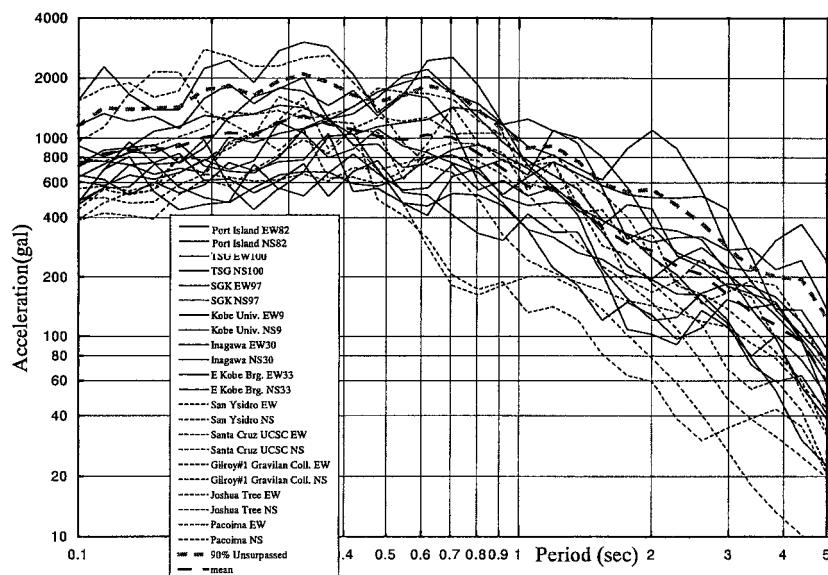


Fig. 4 Adjusted response spectra of observed records to the equivalent hypocentral distance of 12km

earthquake record numbers 4 and 11. Scattering of the response spectra in the short period range is decreased as compared with the original spectra (Figure 3), but in the long period range there is no improvement. Earthquake motion characteristics in the long period range are controlled by the source mechanism and crustal profile surrounding the earthquake fault.

The acceleration response spectra adjusted to the shortest fault distance of 2km also were examined. In intra-plate earthquakes in Japan, the main earthquake energy-releasing portion of the fault is deeper than 2km. This shortest distance therefore means that the observation point is located just above the fault.

### (3) Design Response Spectra

A design response spectrum should be defined by a probabilistic base if there is enough data for stochastic analysis. To define non-exceedance probability the following items must be taken into account:

- 1) The safety of railway facilities must be evaluated from the standpoint of protecting the lives of passengers.
- 2) Damage to a structure causes malfunctioning of the entire rail system.

In the new design standard, 90% of the non-exceedance probability was used to define the design acceleration spectrum, on the assumption that there was a lognormal distribution of the calculated response spectra for each period. The dotted line in Figure 4 shows the acceleration response spectrum with a non-exceedance probability of 90%. On the basis of this line, the design acceleration spectrum is defined by the thick polygonal line shown in Figure 5. We treat this as the mother spectrum defined just above the inland earthquake fault and modify its level based on distance from the fault.

### 3.2 Spectrum I (inter-plate earthquakes)

The response spectrum level that takes into account inter-plate earthquake activities was 1G for the elastic response of structures. This spectrum was revised in the same manner used to define Spectrum II.

#### (1) Earthquake motions analyzed

Recent inter-plate earthquakes of magnitudes larger than 7.4 that occurred near the Japanese archipelago are shown in Figure 1. The records collected consist of 100 components with maximum

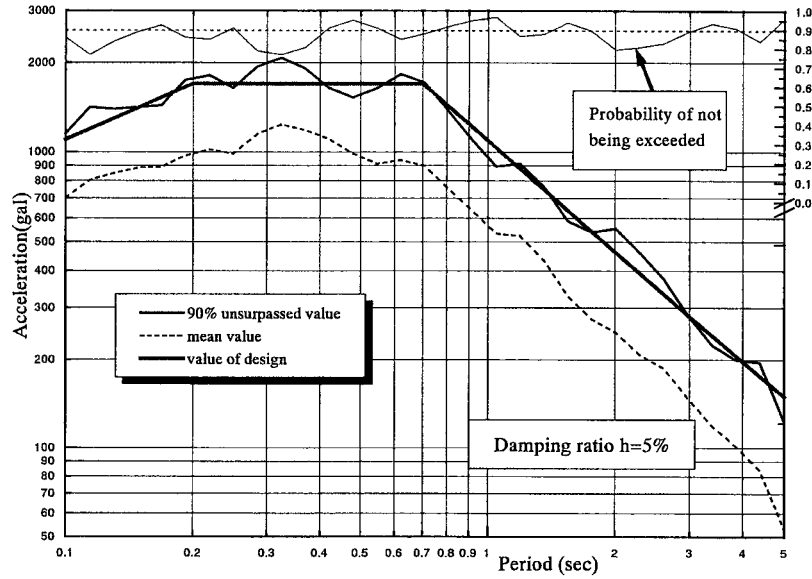


Fig. 5 Comparison of acceleration response spectra, design spectrum, average spectrum and spectrum with 90% non-exceedance probability.

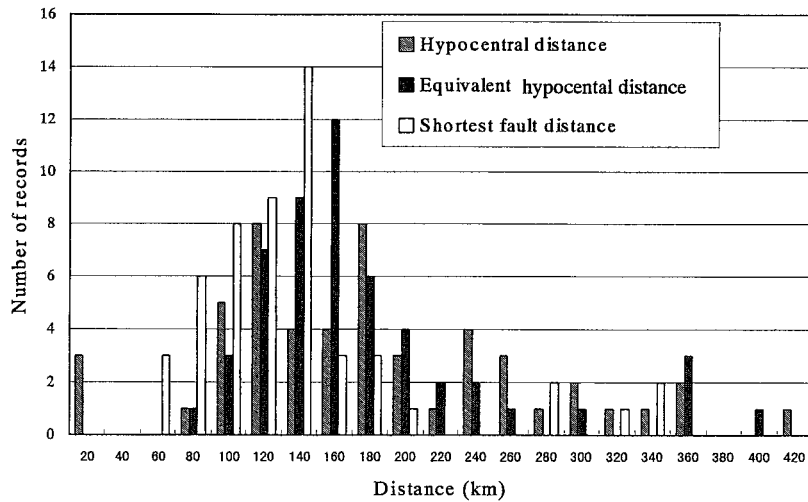


Fig. 6 Distance distribution between the observation point and seismic source

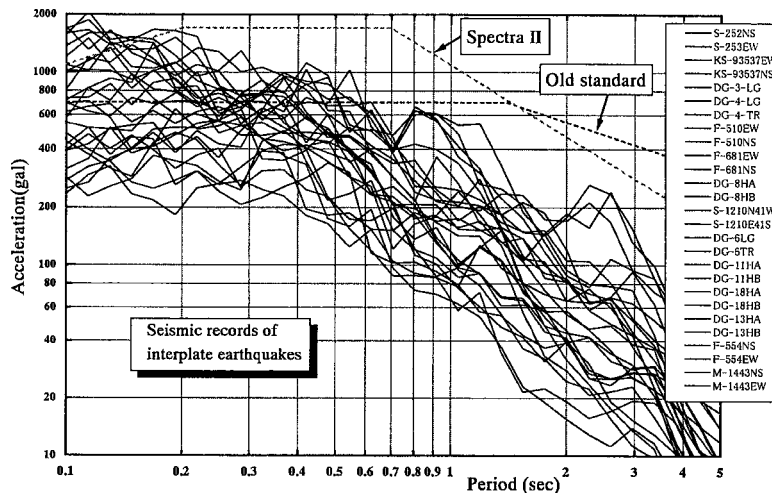


Fig. 7 Acceleration response spectra of observed records of Japanese interplate earthquakes

accelerations of more than 100 gal. Distributions of hypocenters in the observed records are shown in Figure 6. Most data are clustered at hypocentral distances of 100-200 km.

We selected earthquake motions that satisfy the following conditions for statistical analysis;

- An equivalent hypocentral or shortest distance to the earthquake fault of less than 200km
- No conspicuous peaks in the Fourier amplitude spectra.
- Ground condition at the observation points classified as hard ground (of which shear wave velocity is from 350m/sec to 400m/sec).

Twenty-seven records satisfied these conditions. Acceleration response spectra calculated from these records are shown in Figure 7.

## (2) Adjustment of Calculated Response Spectra

The distance to the earthquake fault was used to adjust the calculated response spectra. The concepts of the equivalent hypocentral and shortest distances were used to modify the response spectra. To define Spectrum I, inter-plate earthquakes of magnitude class 8 were targeted. All records of magnitudes less than 8 therefore were adjusted to magnitude 8. The distances to the earthquake fault in Table 3 were used to adjust the response spectra.

The average spectra calculated from the adjusted ones using eqs.(1) and (2) are shown in Figure 8 for cases in which the shortest distance to the earthquake fault was 30km and the equivalent hypocentral distance 80km. The average spectrum for an equivalent hypocentral distance of 80km is larger than that for the shortest distance of 30km. The 80 km equivalent hypocentral distance therefore is comparable to the shortest distance of 20km. The zone

with this shortest distance to a magnitude 8 class inter-plate earthquake fault is located just above the periphery of the fault. In the Kanto and Tokai regions inter-plate earthquake sources are located just below these regions, but the area within the shortest distance of 20km is not wide. In the other regions this distance is classified as being very close area to the earthquake fault.

From this information the design response spectrum that takes into account inter-plate earthquake activities (Spectrum I) is defined by the broken line in Figure 8. In the period range longer than 1.0sec, the spectrum level coincides with Spectrum II for the convenience of design. This spectrum envelopes the adjusted spectra in the period range longer than 0.65 sec but not in the shorter period range. Spectra calculated from the observed motion (Figure 7), however, are enveloped by this spectrum.

This Spectrum I multiplied by the regional modification factor of 0.7 also envelopes the spectra calculated by eqs.(1) and (2) at just above an earthquake fault for an earthquake of magnitude 6.5 and source depth of 10km.

## 4. MODELING OF THE PHASE SPECTRA

Evaluation of the seismic capacities of structures designed using the defined design spectra, requires compatible earthquake motions, and simulation of earthquake motions necessitates both modeling of amplitude and phase characteristics. We propose two methods to define the phase characteristics of design earthquake motion.

The concept of group delay time  $t_{gr}(\omega)$  was used to model the phase spectra of earthquake motion. Group delay time is a derivative of the phase spectrum with respect to circular frequency (Papoulis 1962)<sup>7)</sup>.

$$t_{gr}(\omega) = \frac{d\phi}{d\omega} \quad (3)$$

Its mean value is the central arrival time of ground motion with the frequency component  $\omega$ , and its standard deviation corresponds to the duration of the ground motion concerned. Modeling the group delay time is much easier than direct modeling of the phase.

Table 3. Target distance to the earthquake fault and the earthquake scale used for adjustment

	Closest Distance to Fault		Equivalent hypocentral distance	
	Objective distance (km)	Scale of Earthquake (Mw)	Objective distance (km)	Scale of Earthquake (Mw)
Case1	30	8.0	50	8.0
Case2	50	8.0	80	8.0
Case3	80	8.0	100	8.0

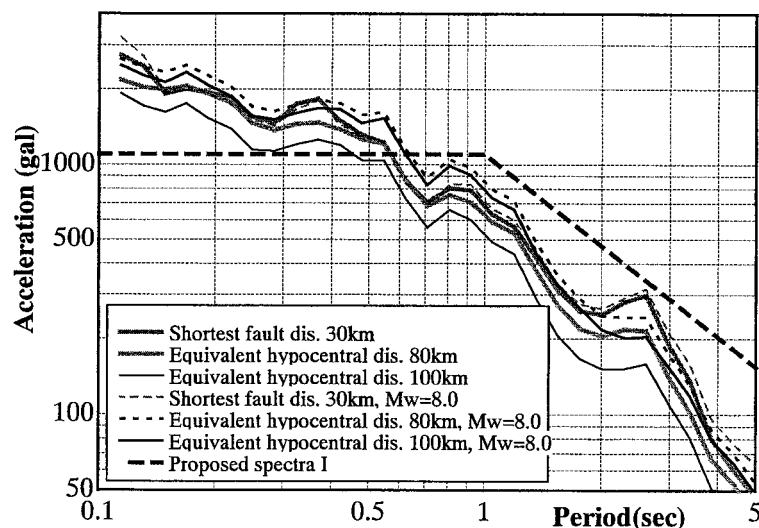


Fig. 8 Comparison of adjusted acceleration response spectra

#### 4.1 Modeling of Group Delay Time for Design Spectrum II

##### (1) Modeling of the Rupture Process of an Earthquake Fault

A fault model of the Haskel type is assumed. The fault plane is divided into  $n \times n$  elements, each of which corresponds to the area of a small event. The motion of the large event  $g_{ol}(t)$  at the observation point is expressed by taking into account the time delay of each small event,  $g_{os}(t)$  (Irikura 1983)<sup>8)</sup>;

$$g_{ol}(t) = \sum_{i=1}^{n_L} \sum_{j=1}^{n_W} g_{os}(t-t_{ij}) + \sum_{i=1}^{n_L} \sum_{j=1}^{n_W} \sum_{k=1}^{(n_D-1)n'} \frac{1}{n'} g_{os}(t-t_{ijk}) \quad (4)$$

in which

$$t_{ij} = \frac{(R_{ij} - R_0)}{V_s} + \frac{\xi_{ij}}{V_r}, \quad t_{ijk} = t_{ij} + \frac{k \tau}{(n_D - 1)n'} \quad (5)$$

where  $\tau$  is the rise time;  $V_s$  the shear wave velocity of the media;  $V_r$  the rupture velocity;  $\xi_{ij}$  the distance between the starting point of rupture and the small event point;  $n_L$ ,  $n_W$ ,  $n_D$  the respective similarity ratios for fault length, width and rise time between the large and small events;  $R_{ij}$  the distance between the representative point of the small event and the observation point; and  $n'$  an arbitrary integer to eliminate any artificial period caused by subdivision of the rise time.

Deconvoluting eq.(4) with respect to the source time function and train of impulses,  $p(t)$ , expressing the rupture process of earthquake fault gives

$$\begin{aligned} p(t) &= \sum_{i=1}^{n_L} \sum_{j=1}^{n_W} \bar{a}_{ij} \delta(t-t_{ij}) + \sum_{i=1}^{n_L} \sum_{j=1}^{n_W} \sum_{k=1}^{(n_D-1)n'} \frac{1}{n'} \bar{a}_{ij} \delta(t-t_{ijk}) \\ &= \sum_{i=1}^N a_i \delta(t-t_i) \quad (6) \\ N &= n_L \times n_W \times (n_D - 1) n' \end{aligned}$$

Because the Fourier amplitude of eq.(6) at zero frequency is proportional to the seismic moment of the earthquake fault, for the case of multiple events the value  $\bar{a}_{ij}$  is assigned as proportional to the seismic moment of each fault. The effect of geometrical damping factor  $1/R_{ij}$  is considered to evaluate  $\bar{a}_{ij}$ . The phase spectrum  $\phi_p(\omega)$  of  $p(t)$  is

$$\phi_p(\omega) = \tan^{-1} \left( \frac{\sum a_i \sin(\omega t_i)}{\sum a_i \cos(\omega t_i)} \right) \quad (7)$$

The group delay time  $t_{gr}^p(\omega)$  of  $\phi(\omega)$  is obtained by differentiating it with respect to the circular frequency,  $\omega$ ;

$$t_{gr}^p(\omega) = \frac{-\sum_{i=1}^N a_i^2 t_i - \sum_{i=1}^{N-1} \sum_{j=i+1}^N a_i a_j (t_j + t_i) \cos\{\omega(t_j - t_i)\}}{\sum_{i=1}^N a_i^2 + 2 \sum_{i=1}^{N-1} \sum_{j=i+1}^N a_i a_j \cos\{\omega(t_i - t_j)\}} \quad (8)$$

##### (2) Modeling of the phase shift caused by local soil conditions

The amplitude characteristic of the frequency transfer function that expresses the effect of local soil conditions is assumed apriori to be  $A_h(\omega)$ . We applied the minimum phase criterion to define its phase spectrum,  $\phi_h(\omega)$ . This assumption is not valid when the seismic wave takes multiple paths between the observation point and base rock. The phase spectrum that expresses the local soil effect is derived from the Hilbert transformation (Papoulis 1962)<sup>9)</sup> which defines the relationship between amplitude and the phase

spectra;

$$\phi_h(\omega) = -\frac{1}{\pi} \int_{-\infty}^{\infty} \frac{\ln(A_h(y))}{\omega - y} dy \quad (9)$$

Differentiating eq.(9) with respect to  $\omega$ , the group delay time  $t_{gr}^h(\omega)$  is

$$t_{gr}^h(\omega) = \frac{1}{\pi} \int_{-\infty}^{\infty} \frac{\ln(A_h(y))}{(\omega - y)^2} dy = \frac{1}{\omega^2} * \{\ln(A_h(\omega))\} \quad (10)$$

in which  $*$  is the symbol expressing convolution.

The phase spectrum of the frequency transfer function from the base rock to ground surface is expressed by the sum of the minimum phase function and the all pass function (Izumi 1990)<sup>9)</sup>. The group delay time of the all pass function nearly coincides with the travel time of the direct wave from the base rock to ground surface. The effect of the group delay time of the all path function therefore is just to shift the arrival time of earthquake motion, and this effect was neglected in the simulation of earthquake motions compatible with design response spectra.

##### (3) Linearity of Group Delay Time

If an earthquake motion is expressed by the convolution of two functions (a function of source and transmitting path,  $p(t)$ , and one of local amplification,  $h(t)$ , the phase of earthquake motion,  $\phi(\omega)$ , is the linear sum of these functions' phases,  $\phi_p(\omega)$  and  $\phi_h(\omega)$ . Because the linearity of the group delay time also is preserved, the group delay time of earthquake motion  $t_{gr}(\omega)$  is expressed as the linear sum of each function's group delay time

$$t_{gr}(\omega) = t_{gr}^p(\omega) + t_{gr}^h(\omega) \quad (11)$$

##### (4) Simulation of Earthquake Motion Compatible with Design Spectrum II

The Fourier amplitude spectra calculated from the observed earthquake motions and the phase spectra obtained by integrating group delay times simulated by using eq.(11) taking into account the fault rupture process and local site condition were used to resimulate the earthquake motions of the 1995 Hyogoken Nambu earthquake. The validity of eq.(11) for estimating the phase spectra was verified by comparing the resimulated earthquake motions with the observed ones (Sato *et al.* 1999)<sup>10)</sup>.

Design earthquake motion compatible with Spectrum II therefore is simulated by using eq.(11) to define phase spectra. The assumed earthquake fault is a vertical one with the size of  $40 \times$

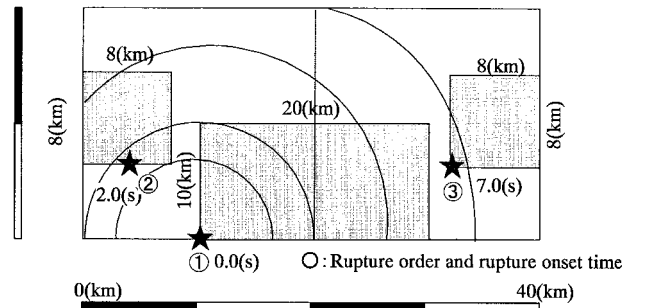


Fig. 9a Example of the rupture fault model used in the analyses

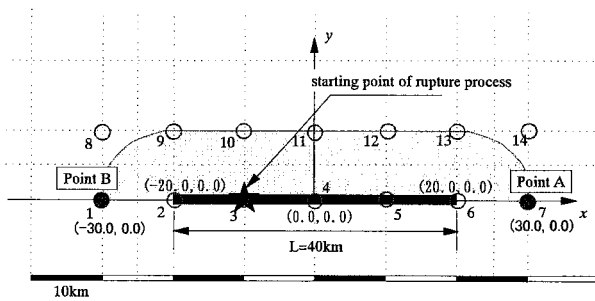


Fig. 9b Relative position between the observation points and fault

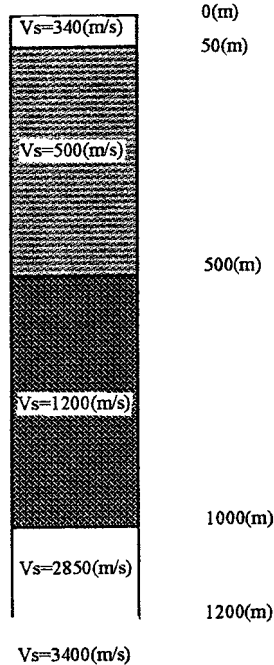
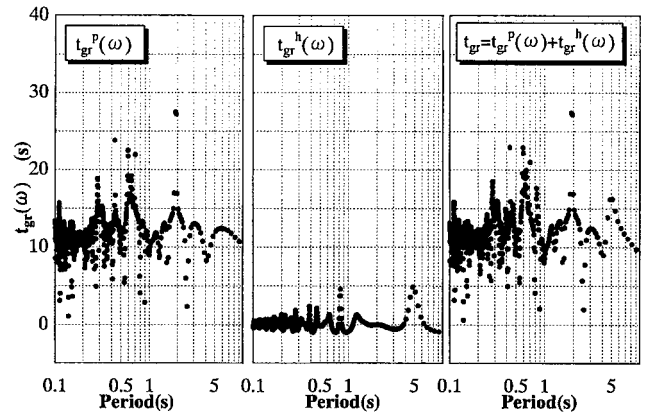


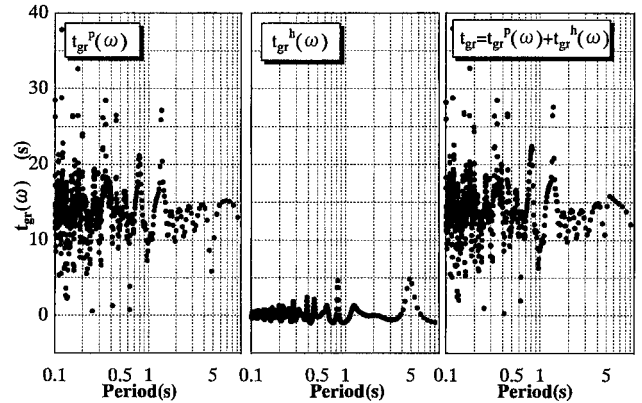
Fig. 10 Ground profile used to evaluate local soil effect

20(km). In the parameter studies we selected several combinations of the starting point of fault rupture and distribution of asperity because these values strongly affect the phase characteristics of earthquake motion. We considered three types of asperity distributions and three cases of rupture starting points. The size and distribution of asperity were defined from seismological research results (Somerville 1993)<sup>11)</sup>. From the parameter studies, we selected the combination of asperity distributions and starting points of fault rupture, shown in Figure 9a, as the most severe fault rupture model to generate design phase spectrum. Fourteen observation points around the fault (Figure 9b) are considered to define the design earthquake motion compatible with design Spectrum II. The procedure used to simulate earthquake motion compatible with the design response spectrum is given in the Appendix. The depth of the base rock is assumed to be 1500m and the shear wave velocity  $V_s=3400(\text{m/s})$ . The amplitude spectrum expressing local soil condition  $A_s(\omega)$  is calculated by the multi reflection theory of one dimensional SH wave. Ground profile used for the calculation is shown in Figure 10.

Representative results of the parameter analyses are shown in Figures 11 and 12, in which the group delay times and simulated earthquake motions compatible with Spectrum II respectively are given. Point A is located in the direction of rupture propagation,



(a) Group delay time at point A



(b) Group delay time at point B

Fig. 11 Simulated group delay times at points A and B

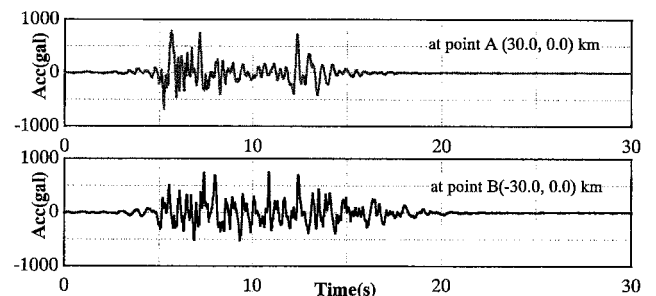


Fig. 12 Earthquake motions compatible with design spectrum II

and point B in the opposite direction. Scattering of the group delay time of the train of impulses is small for the observation point located in the direction of rupture propagation (point A), increasing in the opposite direction (point B). The directivity of rupture propagation shows clearly in the group delay time. This phenomenon was confirmed in the simulated earthquake motions (Figure 12). Even when the same response spectrum is used, the waveform is strongly affected by the relative position of the observation point and the rupture configuration. If the observation point is located in the direction of rupture propagation, wave energy is concentrated over a short period. In the opposite direction, however, the duration of earthquake motion lengthens.

The ductility demand spectrum was used to analyze the effect of these earthquake motion characteristics on the dynamic analyses of structure systems. This spectrum was obtained through nonlin-

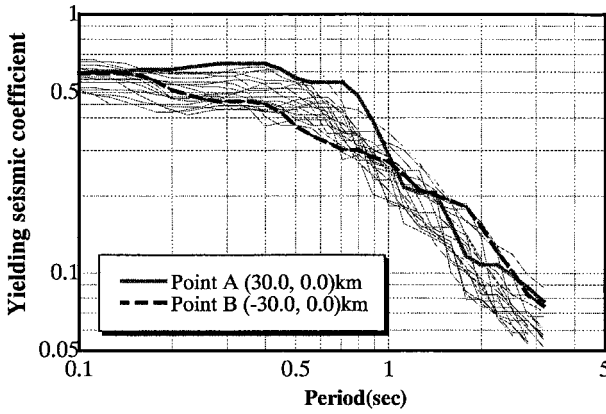


Fig. 13 Strength demand spectra for earthquake motions compatible with design spectrum II ( $\mu=4$ )

ear dynamic response analyses of a single degree of freedom system. The yield seismic coefficient of the SDF is controlled until the SDF response reaches the targeted ductility. The chart that expresses the relationship between the yield seismic coefficient and elastic natural period is called the ductility demand spectrum, in which the targeted ductility is a parameter. The hysteresis model used in the analyses is the bi-linear type proposed by Clough (1966). The second stiffness was selected as 5% of the first, and a 5% damping coefficient assigned. Results for a ductility 4 are shown in Figure 13. The thin lines are ductility demand spectra calculated from simulated earthquake motions compatible with Spectrum II using the phase spectra of twenty observed earthquake motions. The ductility demand spectrum for the earthquake motion at point A envelopes all twenty results. Because this spectrum has a very smooth nature in all the frequency ranges we designated this earthquake motion as the design earthquake motion compatible with Spectrum II.

#### 4.2 Modeling of Group Delay Time for Design Spectrum I

##### (1) Average Group Delay Time and Its Standard Deviation

Wavelet analysis often is used to determine the nonstational characteristic of earthquake motion in the time and frequency domains because resolution in these domains is guaranteed by the uncertainty criterion.

The discrete wavelet transformation of function  $x(t)$  and its inverse transformation have been defined by (Yamaguchi, 1990)<sup>12)</sup>;

$$a_{j,k} = \int_{-\infty}^{\infty} \psi_{j,k}^* \cdot x(t) dt \quad (12)$$

$$x(t) = \sum_j x^{(j)}(t) = \sum_j \sum_k a_{j,k} \cdot \psi_{j,k}(t) \quad (13)$$

$$\psi_{j,k}(t) = 2^{j/2} \cdot \psi(2^j t - k) \quad j, k : \text{integer} \quad (14)$$

in which the value with the sign \* expresses the complex conjugate of the original value,  $\psi(t)$  the wavelet function,  $j$  is the scale factor, and  $k$  the factor expressing the time shift. If the inverse wavelet transformation exists,  $\psi(t)$  is called the analyzing wavelet. Although there are several ways to define this function, we used the method of Meyer (Meyer 1989)<sup>13)</sup> to compose  $\psi(t)$ . The

Fourier transformation of  $\psi_{j,k}(t)$  has a compact support for each scale factor  $j$  (named the  $j$ th compact support) defined by

$$\{2^j / 3T_d \leq f \leq 2^{j+2} / 3T_d\} \quad (15)$$

in which  $T_d (=N \Delta t, N$ : number of data,  $\Delta t$ : sampling interval) is the duration of earthquake motion. As seen from eq.(15), if scale factor  $j$  becomes large, the treating frequency range shifts to the high frequency region.

For all observed earthquake motions with a sampling interval of 0.01(sec) zero data were added until the total number of sampling data for each earthquake motion,  $N$ , became 131071 ( $=2^{17}$ ). The wavelet transformation of each earthquake motion  $x(t)$  was used to decompose each time history of earthquake motion to a component time history of each scale factor  $j$  ( $j=1 \sim 17$ ). We call this the  $j$ th component time history,  $x^{(j)}(t)$ . Based on the definition of  $x^{(j)}(t)$  given in eq.(13) the frequency band of this time history is limited, as defined by eq.(15).

The group delay time of this time history,  $t_{gr}^{(j)}(\omega)$ , was calculated and its mean,  $\mu_{igr}^{(j)}$ , and standard deviation,  $\sigma_{igr}^{(j)}$ , on the  $j$ th compact support obtained from eqs.(16) and (17):

$$\mu_{igr}^{(j)} = \frac{\sum_{i=1}^{N^{(j)}} t_{gr}^{(j)}(\omega_i)}{N^{(j)}} \quad (16)$$

$$\sigma_{igr}^{(j)} = \sqrt{\frac{1}{N^{(j)}} \sum_{i=1}^{N^{(j)}} (t_{gr}^{(j)}(\omega_i) - \mu_{igr}^{(j)})^2} \quad (17)$$

in which  $j=1,2,\dots,17$ ,  $N^{(j)}$  is the number of time history data at the  $j$ th scale factor defined by  $N^{(j)}=2^j$ , and  $t_{gr}^{(j)}(\omega_i)$  the group delay time of the  $j$ th component time history at a circular frequency of  $\omega_i$ , defined by equation (18);

$$t_{gr}^{(j)}(\omega_i) = \frac{d\phi}{d\omega} = - \frac{\phi(\omega_i) - \phi(\omega_{i+1})}{\Delta\omega} \quad (18)$$

##### (2) Regression Equations of Group Delay Time

Existing data sets for the observed earthquake motions are used to calculate the group delay time of each earthquake motion. The attenuation relationships of the mean and standard deviation of the group delay time on each compact support are obtained as functions of earthquake magnitude and epicentral distance.

Data sets of the earthquake motions analyzed are from the Off Southwest Hokkaido earthquake (1993, M7.8), the Off East Hokkaido earthquake (1994, M8.1), the Off Sanriku earthquake (1994, M7.5), and the Hyogoken Nambu earthquake (1995, M7.2).

The starting time of rupture at the earthquake fault was selected as the origin of the time history of earthquake motion. The theoretically calculated travel time of the S wave from the initial rupture point to the observation site is added to the trigger time. In standard seismic design procedures the period range concerned is 0.1 ~ 5 sec. Regression equations  $\mu_{igr}^{(j)}$  and  $\sigma_{igr}^{(j)}$  for  $j=6 \sim 15$  therefore were developed as functions of earthquake magnitude  $M$  and epicentral distance  $\Delta$  (km);

$$\mu_{igr}^{(j)} = \alpha_1^{(j)} \times 10^{\beta_1 M} \times \Delta^{\gamma_1}, \quad \sigma_{igr}^{(j)} = \alpha_2^{(j)} \times 10^{\beta_2 M} \times \Delta^{\gamma_2} \quad (19)$$

in which  $\alpha_1^{(j)}$ ,  $\alpha_2^{(j)}$ ,  $\beta_1^{(j)}$ , and  $\beta_2^{(j)}$  are regression coefficients on the  $j$ th support.

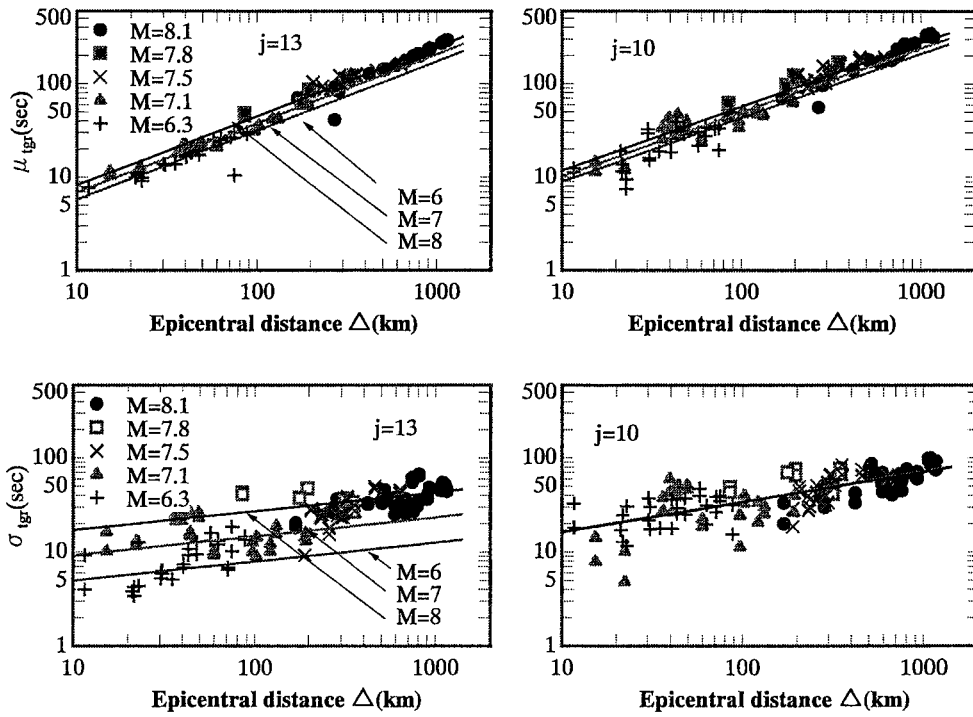


Fig. 14 Relationship between the epicentral distance  $\Delta$  and the mean and standard deviations of group delay time on scale factor  $j=10,13$

Table 4. Regression analyses results

$j$	$a_1$	$a_2$	$\beta_1$	$\beta_2$	$\gamma_1$	$\gamma_2$	correlation coeff	
							$\mu$	$\sigma$
7	1.011	27.708	0.0	0.0	0.864	0.203	0.86	0.41
8	0.830	14.584	0.040	0.0	0.790	0.337	0.96	0.71
9	0.543	17.968	0.086	-0.030	0.700	0.344	0.85	0.75
10	0.806	8.451	0.060	-0.005	0.686	0.321	0.97	0.73
11	0.850	2.970	0.026	0.016	0.764	0.366	0.98	0.77
12	0.511	0.392	0.058	0.143	0.744	0.295	0.99	0.83
13	0.367	0.0790	0.077	0.267	0.739	0.201	0.99	0.87
14	0.330	0.0572	0.081	0.287	0.742	0.239	0.99	0.81
15	0.0443	0.0106	0.256	0.439	0.591	0.204	0.97	0.79

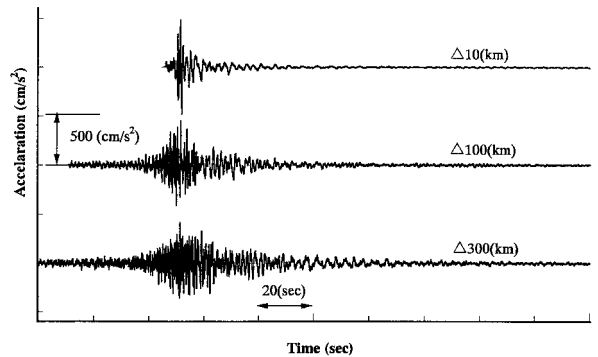


Fig. 15 Earthquake motions compatible with design spectrum I

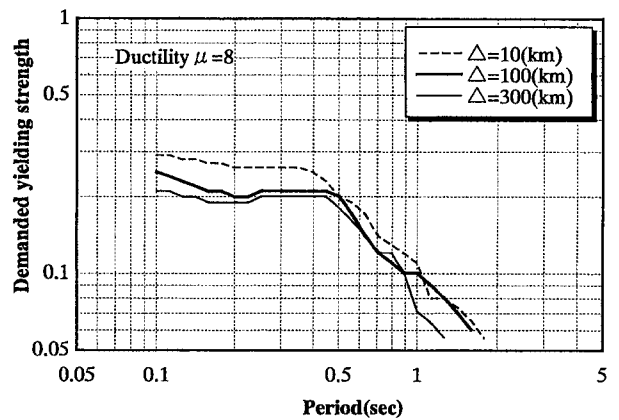
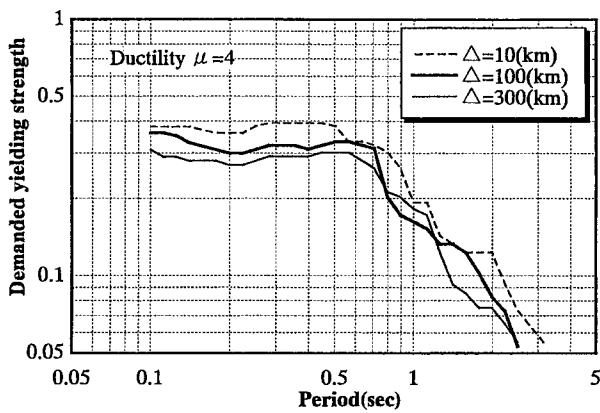


Fig. 16 Ductility demand spectra for earthquake motions shown in Figure 15

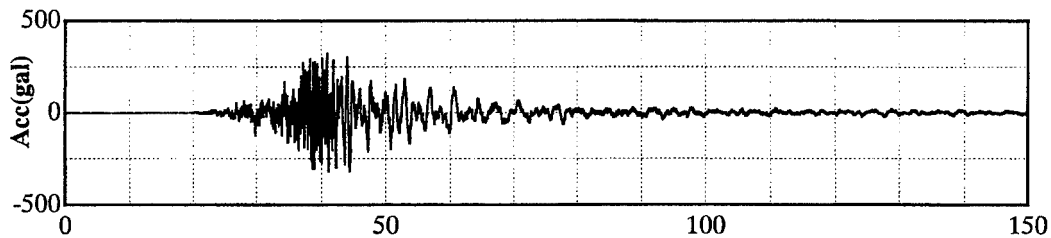


Fig. 17 The design earthquake motion compatible with design spectrum I

Regression analyses results are given in Table 4, and some are shown in Figure 14. Values of  $\mu_{igr}^{(j)}$  and  $\sigma_{igr}^{(j)}$  increase as the epicentral distance increases, especially in the longer period range (for a small  $j$  value) because  $\alpha_1$  and  $\alpha_2$  values are increases as the  $j$  value decreases. The effect of epicenter distance on  $\mu_{igr}^{(j)}$  and  $\sigma_{igr}^{(j)}$  is almost same because  $\gamma_1$  and  $\gamma_2$  have constant values for all  $j$  values. The effect of earthquake magnitude on  $\mu_{igr}^{(j)}$  and  $\sigma_{igr}^{(j)}$  is rather small comparing with that of epicenter distance because values of  $\beta_1$  and  $\beta_2$  are small. The values of  $\beta_1$  and  $\beta_2$  are related to shorter period motions because those values increase as the  $j$  value increases but the values of  $\alpha_1$  and  $\alpha_2$  are related to longer period motions.

### (3) Simulation of Earthquake Motion Compatible with Design Spectrum I

The values of  $\mu_{igr}^{(j)}$  and  $\sigma_{igr}^{(j)}$  on the  $j$ th compact support were obtained from eq.(19) for an earthquake of magnitude 8.0 and three epicentral distances (10, 100, 300km) used to simulate earthquake motions compatible with design Spectrum I (Figure 8). Because the frequency range of each compact support  $j$  defined by eq.(15) is overlapping with that of neighboring compact supports  $j-1$  and  $j+1$ , we assume that the frequency range  $2^{j-1}/T \leq f \leq 2^j/T$  is effective to generate the group delay time in the compact support  $j$ . A sample group delay time on the  $j$ th compact support for each epicentral distance is simulated by generating a random value based on a normal distribution  $N(\mu_{igr}^{(j)}, \sigma_{igr}^{(j)})$  although Nigam (1982)<sup>14)</sup> derived a probability density function for group delay time different from the Gauss distribution. The phase spectrum on the  $j$ th support is obtained by integrating this sample group delay time. To guarantee the continuity of phase spectrum the initial value of phase in the frequency range  $2^{j-1}/T \leq f \leq 2^j/T$ , which is the representative frequency range of compact support  $j$ , is assigned as the final phase of the frequency range  $2^{j-2}/T \leq f \leq 2^{j-1}/T$  which is the representative frequency range of the compact support  $j-1$ . Simulated earthquake motions compatible with design Spectrum I (see Appendix) are shown in Figure 15. This design spectrum is defined by taking into account only the activity of inter-plate earthquakes. The epicentral distance therefore is more than 30-40km, but we added a case of a 10km epicentral distance. As the epicentral distance increases the duration lengthens, and longer period motion predominates.

Ductility demand spectra (Figure 16) were calculated from the simulated earthquake motions. Although the same elastic response spectrum was used to simulate the earthquake motions, the strong effect of epicentral distance can be seen on the elastoplastic structural response characteristics. A short epicentral distance requires large ductility, whereas the demand decreases as the epicentral distance increases.

For design purpose it is not practical to use a sample earthquake motion compatible with Spectrum I because the time history characteristic of a simulated earthquake motion is strongly affected by the random nature of a generated group delay time. We therefore simulated several tens of design earthquake motions compatible with Spectrum I by supposing earthquake ground motions with magnitude  $M=8$  at the epicentral distance  $\Delta=80$ (km). From these an earthquake motion (Fig. 17) was selected as the standard earthquake motion to be used for the design purpose because it has a smooth shape of ductility demand spectra.

## 5. CONCLUSION

We introduced the concept of design earthquake motions as defined in the design standards for Japanese railway facilities, in particular the procedures used to define design acceleration spectra and to simulate earthquake motions compatible with the design spectra.

The following findings were obtained:

- 1) Three types of design acceleration spectra were defined in the seismic design standards for Japanese Railway Facilities.
- 2) The concept of group delay time was used to model the phase spectra of earthquake motions. A method to simulate phase spectra of earthquake motions at near source regions was developed by taking into account the effect of rupture process of earthquake faults and local soil conditions.
- 3) From data sets of observed earthquake motions and the wavelet algorithm, the mean group delay time and standard deviation on the compact support of the Meyer wavelet were expressed as functions of earthquake magnitude and epicentral distance (regression equations). We developed a method to simulate a sample phase spectrum for an inter-plate earthquake motion based on the regression equations.
- 4) Using the simulated sample phase spectrum a method to simulate earthquake motions compatible with the design response spectrum was developed. Its suitability for design purposes was investigated using ductility demand spectra.

## APPENDIX

The method to simulate earthquake motions compatible with design spectra is summarized. The simulated phase spectrum on the  $j$ th compact support  $\phi^{(j)}(\omega)$  is used to simulate an earthquake motion compatible with the response spectrum. To do this, an initial Fourier amplitude spectrum  $A_{in}(\omega)$  is needed. This is assumed to be given by the velocity response spectrum with a zero damping constant converted from the design acceleration

response spectrum given by

$$A_{int}(\omega) = \left( \frac{\beta}{1 + \alpha h} + \gamma \right) \omega S(\omega, 0.05), \quad (20)$$

in which  $S(\omega, 0.05)$  is the targeted design spectrum with 5% damping,  $h$  the damping constant, and  $\alpha$ ,  $\beta$  and  $\gamma$  are given parameters (Kawashima and Aizawa, 1986)<sup>15)</sup>

The initial Fourier amplitude of the  $j$ th compact support  $A^{(j)}(\omega)$  is assumed to coincide with the initial Fourier amplitude  $A_{int}(\omega)$  in the frequency range  $\{2^{j-1}/T_d \leq f \leq 2^j/T_d\}$  and to be zero outside of this region; i.e., in the frequency regions  $\{2^j/3T_d \leq f < 2^{j+1}/T_d\}$  and  $\{2^j/T_d < f \leq 2^{j+2}/3T_d\}$ . A  $j$ th component time history can be simulated using  $\phi^{(j)}(\omega)$  and  $A^{(j)}(\omega)$ . Earthquake motion of the first step is obtained by summing up all the component time histories. Because the calculated response spectrum based on first step earthquake motion does not coincide with the design response spectrum, we modified the amplitude of the initial Fourier amplitude,  $A_m(\omega)$ , at the circular frequency,  $\omega$ , by multiplying the ratio  $r(\omega)$  of the design response spectrum and calculated response spectrum. Assuming the calculated  $r(\omega) A_m(\omega)$  as the new initial Fourier amplitude of earthquake motion and using the original phase spectrum of the  $j$ th component  $\phi^{(j)}(\omega)$ , the earthquake motion of the second step can be simulated. Repetition of this process until the ratio  $r(\omega)$  nearly equals 1.0, gives simulated earthquake motion compatible with the design response spectrum.

## REFERENCES

- 1) Rika Nenpyo (Chronological Scientific Tables 2001), pp.800-831, National Astronomical Observatory, Japan. Maruzen Co., Ltd., 2000
- 2) JSCE, 'Proposal on earthquake resistance for civil engineering structures', Special task committee of earthquake resistance of civil engineering structures, Japan, (1996)
- 3) Ministry of Transportation and Railway Research Institute, 'Seismic Design Standards for Railway Facilities', Marzen, (1999), (in Japanese).
- 4) Y. Fukushima, 'Empirical prediction for strong ground motion reflected on theoretical backgrounds of source and propagation of seismic wave', *ORI Report 93-07*, Ohsaki Research Institute, (1994), (in Japanese).
- 5) S. Ohno and K. Takahashi, 'Evaluation of strong-motion attenuation relation using near-source data in California', *Proc. of the 9th Japan Earthquake Engineering Symposium*, (1994), (in Japanese).
- 6) H. Wang, Y. Murono and A. Nishimura, 'On evaluation of ground motion near seismic faults based on strong seismic records', *Proc. of the 2nd Urban Earthquake Disaster Symposium*, (1997), (in Japanese).
- 7) A. Papoulis, 'The Fourier integral and its application', McGRAW-Hill, (1962).
- 8) K. Irikura, 'Semi-empirical estimation of strong ground motions during a large earthquake', *Bulletin of Disaster Prevention Research Institute*, Kyoto University, Vol.33, Part2, No.297, 63-104, (1983).
- 9) M. Izum, S. Kurita, Y. Endo, J. Tobita and T. Hanzawa, 'Study on causality of transfer functions and components of causal transfer functions in systems of seismic wave propagation in soil', *J. of Structure Construction Engineering, AIJ.*, No.412, 31-41, (1990), (in Japanese)
- 10) T. Sato, Y. Murono and A. Nishimura, 'Modeling of phase characteristics of strong earthquake motion', *J. Struct. Mech. Earthquake Eng., JSCE*, No.612/I-46, 201-213, (1999), (in Japanese)
- 11) P. G. Somerville, K. Irikura, S. Sawada, Y. Iwasaki, M. Tai and M. Fushimi, 'A study on empirical modeling of slip distribution on faults', *Proc. of the 22th JSCE Earthquake Engineering Symposium*, 291-294, (1993).
- 12) M. Yamaguchi and M. Yamada, 'Wavelet analysis', *Science*, Vol.60 No.6, 398-405, (1990) (in Japanese).
- 13) Y. Meyer, 'Wavelets and operator', Cambridge University Press, (1992).
- 14) N. C. Nigam, 'Phase properties of a class of random process' *Earthquake Engineering and Structural Dynamics*, Vol. 10, 711-714, (1982).
- 15) K. Kawashima, K. Aizawa and K. Takahashi, 'Attenuation of peak ground motion and absolute acceleration response spectra' *Proc. of 8th World Conference on Earthquake Engineering*, Vol.II, 257-264, (1984).